Effect of Rotation on Surface Tension Driven Flow During Protein Crystallization

P. Bhattacharjee[1] and D. N. Riahi[2]

[1]Department of Aeronautical and Astronautical Engineering, 306 Talbot Laboratory, 104 S. Wright St., University of Illinois, Urbana, Illinois 61801 USA

[2]Department of Theoretical and Applied Mechanics, 216 Talbot Laboratory, 104 S. Wright St., University of Illinois, Urbana, Illinois 61801 USA

Abstract

Effect of rotation on surface tension gradient driven flow, which is also known as Marangoni convective flow, during protein crystallization is modelled and studied computationally under microgravity conditions, where the surface tension gradient force is the main significant driving force. The axis of the externally imposed rotation, which is assumed to be either parallel or anti-parallel to the gravity vector, is assumed to be inclined at an angle γ with respect to the axis of the crystal. In addition to the angle γ, the main parameters are the solutal Marangoni number M_c, representing the surface tension gradient force and the Taylor number T_a representing the rotational effect. The numerical computations for various values of the parameters and low gravity levels indicated non-trivial competing effects, due to surface tension gradient, centrifugal and Coriolis forces, on the flow adjacent to the protein crystal interface and the associated solute flux. In particular, for given values of M_c, certain values of T_a were detected where the Sherwood number, representing the convective solute flux, and the convective flow effects are noticeably reduced. These results can provide conditions under which convective flow transport during the protein crystallization approaches the diffusion limited transport, which is desirable for the production of higher quality protein crystals.

1. Introduction

It is known that space environment under microgravity condition has the advantage over the earth environment for the production of higher quality crystals since at least the component of the undesirable convective flow due to the buoyancy force is negligible under the microgravity condition of the space environment. A number of experiments involving protein crystal growth that have been carried out in space under microgravity condition, have been able to produce certain types of crystals that were relatively larger and better ordered as compared to those grown on earth under normal (earth) gravity ($1g_0$ –level) condition [1-4]. The main motivation for growing protein crystals in space has been to achieve diffusion controlled growth condition, which was thought to produce higher quality crystal. However, there have also been a number of flight experiments that produced crystals with no noticeable improvement in the quality and internal structure as compared to those grown under the normal gravity on earth. One main problem due to the space environment under the microgravity condition has been the dominance of the effect of surface tension gradient force, which is undesirable and can adversely affect the crystal-melt interface. Although this problem is difficult to be examined quantitatively at present due to the lack of sufficient information about the surface tension and its precise variation with respect to the solute concentration, qualitative information about ways that Marangoni effect can be reduced noticeably, is of value. The present investigation seeks to determine such information for the case where the protein crystal growth in a microgravity environment is under a rotational constraint. We have detected some interesting results about the beneficial effects of the external constraint of rotation. In particular, we found certain values of the rotation rate under which the effect of the surface tension gradient force is reduced noticeably.

In the engineering applications, a number of studies already documented the beneficial effects of rotation, under some conditions, on the growth of crystals other than those due to proteins. Lie et al. [5-6] studied centrifugal pumping with applications to semiconductor crystal growth and silicon crystal growth in float zone processes. Riahi [7-9] investigated asymptotically nonlinear compositional convection during alloy solidification in a high gravity environment, where the solidification system was

subjected to an inclined rotational constraint, and determined range of values for the centrifugal and Coriolis parameters under which buoyancy driven convection may be as weak as possible. The results of such previous investigations for the alloys and semiconductor crystal growth cases motivated us to undertake the present study of the effect of rotation on the protein crystal growth.

The problems of convective flows, subjected to the surface tension gradient force, are of considerable interest in geophysics and engineering [10]. A number of nonlinear studies have been carried out in the past [11-20]. The only work that takes into account the effects Coriolis force in a Benard-Marangoni type convection in a rotating fluid is apparently that of Riahi [21] who studied theoretically the weakly nonlinear case near the onset of motion and found, in particular, some stabilizing effect of the Coriolis force on the flow pattern.

In regard to the effects of the surface tension gradient force on flows during non-protein crystal growth, some results have been determined for flow in a circular cylindrical float zone [22] and for flow during a realistic float zone crystal growth [23]. For flow during protein crystal growth, very few investigations have been done sofar to study the Marangoni effect [24]. Resenberger [25] have made some qualitative points about the Marangoni effects on flow during protein crystal growth. Monti and Savino [26-27] investigated numerically some modeling aspects of fluid mechanics of vapour diffusion systems and studied qualitatively the Marangoni effects that could exist in drops and around growing crystals.

The present paper investigates computationally and for the first time the effect of rotation on surface tension driven flow during protein crystallization under different microgravity environments. Our computational modeling and procedure is similar to that used by Ramachandran [28] for buoyancy driven convection during protein crystal growth and in the absence of rotation. Due to the complexity of the present problem, which is compounded by the presence of the externally imposed inclined rotation, we have restricted our study to the simplest case of a planar model for the protein system

where the governing system of equations is satisfied and the effects of centrifugal force, Coriolis force and the surface tension gradient force are all taken into account. This is our first study of the surface tension driven convection during protein crystal growth and under the inclined rotational effect. Extension to fully three-dimensional model is beyond the scope of the present study but is planned to be carried out by the present authors in near future.

2. Governing System

We consider a small cylindrical crystal growing in a cylindrical chamber whose axis coincides with that of the crystal. We employ the modeling data similar to those used in [28] for the protein crystal, the chamber and the fluid within the chamber boundary and the crystal. Hence, diameter size of the crystal is chosen to be 0.1 cm, length of the height L of the crystal is taken as 0.1 cm, and the crystal is suspended with its center 0.25 cm from the bottom of the chamber. The values of the kinematic viscosity ν, solute diffusivity D and density ratio $\Delta\rho/\rho_\infty \equiv(\rho_\infty - \rho_i)/\rho$, are taken [28] respectively as 0.01 cm^2/s, 0.000001 cm^2/s and 0.01. Here ρ_i is the density at the crystal-melt interface, which is assumed to be a constant, and ρ_∞ is the reference density of the fluid away from the crystal interface.

Following [28], the moving boundary of the crystal can safely be ignored since the crystal growth velocity is sufficiently slow. No-slip conditions for flow velocity are used on the crystal surface and on the container's solid boundary in contact with the fluid, while impermeable and free surface conditions, where viscous shear stresses balance the surface tension gradient, are assumed at the top surface of the fluid, which is not in contact with the container's boundary. Additional boundary conditions for the solute concentration C are that $C=C_i$ on the crystal interface and $C=C_\infty$ at the container's boundary in contact with the fluid, where C_∞ is assumed to be a constant. As explained in [28], the dependence of C_i on the growth system is generally unknown, at present, for most of the protein growth systems, and, thus, C_i is also taken as a constant. Adopting

Boussinesq approximation [29], the density difference $\Delta\rho$ is then directly proportional to the difference in the solute concentration.

The governing equations for momentum, continuity and solute concentration are given by

$$\rho_\infty(\partial/\partial t+ \mathbf{u}.\nabla)\mathbf{u}= -\nabla P+\rho_\infty\nu\nabla^2\mathbf{u}+(\rho-\rho_\infty)\mathbf{F}_g+(\rho-\rho_\infty)\mathbf{F}ce +\rho_\infty\mathbf{F}_{co}, \quad (1)$$

$$\nabla.\mathbf{u}=0, \quad (2)$$

$$(\partial/\partial t+ \mathbf{u}.\nabla)C=D\nabla^2C, \quad (3)$$

where **u** is the velocity vector, t is the time variable, P is the pressure and ρ is the fluid density. The expressions for the centrifugal $\mathbf{F}_{ce}$, Coriolis $\mathbf{F}_{co}$ and gravity $\mathbf{F}_g$ forces per unit mass will be given shortly. The crystal growth system is assumed to be rotating at some constant angular velocity $\boldsymbol{\Omega}$ about the rotation axis, which considered to be either anti-parallel or parallel with respect to the normal gravity vector. Figure 1(a) provides a planar view of the geometry of the crystal growth system and the planar coordinate system xoy, where the positive x-direction makes, in general, an angle γ with respect to the rotation axis, shown with a dash-dot line, which is in the xoy-plane, and z-axis, which is not shown in the figure 1a, is perpendicular to the plane of xoy and has a right-handed sense. The x-axis is parallel to the axes of crystal and the chamber, and the free surface of the fluid is assumed to be flat and perpendicular to the x-axis. For $0\leq\gamma<90°$, the rotation vector $\boldsymbol{\Omega}$ is assumed to be anti-parallel to the normal gravity vector, while $\boldsymbol{\Omega}$ is assumed to be parallel to the normal gravity vector for $90°\leq\gamma<180°$. The coordinate system, which is assumed embedded in the crystal growth system, is, thus, rotating about the rotation axis. As provided in (1) in the rotating coordinate system, the momentum equation contains terms due to inertial, pressure gradient, viscous, buoyancy, centrifugal and Coriolis forces. The expression for the radius vector **R** shown in the figure 1a can be written in terms of γ, x, y and angle θ, also shown in the figure 1a, as

$$\mathbf{R}=R_x\,\mathbf{x}+R_y\,\mathbf{y}, \tag{4a}$$

where **x** and **y** are unit vectors along positive x- and y-directions,

$$R_x=-r_0\sin\gamma+x[1-\cos(\gamma-\theta)\cos\gamma/\cos\theta],\ R_y=r_0\cos\gamma+y[1-\cos(\gamma-\theta)\sin\gamma/\sin\theta]. \tag{4b}$$

Here r_0 is the magnitude of vector $\mathbf{r}_0$ shown in the figure 1a. Denoting the rotation vector by $\boldsymbol{\Omega}$, the centrifugal, Coriolis and gravity forces per unit mass are given by

$$\mathbf{F}_{ce}=\boldsymbol{\Omega}\times\boldsymbol{\Omega}\times\mathbf{R},\ \mathbf{F}_{co}=2\mathbf{u}\times\boldsymbol{\Omega},\ \mathbf{F}_g=-g\cos\gamma\mathbf{x}+g\sin\gamma\mathbf{y}, \tag{5}$$

where $g=ng_0$ is acceleration due to gravity, g_0 is the normal (earth) acceleration due to gravity (981.0 cm/s^2) and n denotes the gravity level used in the present study.

The governing equations (1)-(3) and the boundary conditions are then non-dimensionalized using L, ν/L, L^2/ν, ΔC and $\rho_\infty\nu^2/L^2$ as scales for length, velocity, time, solute concentration and pressure, respectively. The non-dimensionalized forms of the equations and the boundary conditions are then

$$D\mathbf{u}/Dt=-\nabla P+\nabla^2\mathbf{u}+\mathbf{S},\ D/Dt\equiv(\partial/\partial t+\mathbf{u}.\nabla), \tag{6}$$

$$\nabla.\mathbf{u}=0, \tag{7}$$

$$D\phi/Dt=(1/S_c)\nabla^2\phi, \tag{8}$$

$$\mathbf{u}=0 \text{ on the crystal and on the container boundaries,} \tag{9}$$

$$\phi=0 \text{ on the container's boundary,} \tag{10}$$

$$\phi=-1 \text{ on the crystal surface,} \tag{11}$$

and on the free surface

$$u=0,\ \partial v/\partial x+\partial u/\partial y =(M_c/S_c)\partial C/\partial y,\ \partial w/\partial x+\partial u/\partial z =(M_c/S_c)\partial C/\partial z,\ \partial C/\partial z=0. \qquad (12)$$

Here

$$\mathbf{S}=(S_x, S_y, S_z), \qquad (13a)$$

$$S_x =T_a\,[\Delta\rho/(4\rho_\infty)](-R_y \sin\gamma\cos\gamma+R_x \sin^2\gamma)\phi - \sqrt{T_a}\,(\sin\gamma)w-(G_r\cos\gamma)\phi, \qquad (13b)$$

$$S_y=T_a[\Delta\rho/(4\rho_\infty)](-R_x \sin\gamma\cos\gamma +R_y \cos\gamma)\phi +\sqrt{T_a}\,(\cos\gamma)w-(G_r \sin\gamma)\phi, \qquad (13c)$$

$$S_z =\sqrt{T_a}(-v\cos\gamma +u\sin\gamma), \qquad (13d)$$

and the Boussinesq approximation implies that

$$(\rho-\rho_\infty)=(\Delta\rho)\phi,\ \phi\equiv(C-C_\infty)/\Delta C,\ \Delta C\equiv C_\infty - C_i. \qquad (14)$$

In addition, $S_c =\nu/D$ is the Schmidt number, which has the value of 10000.0 in the present study, $T_a=4\Omega^2L^4/\nu^2$ is the Taylor number, $G_r =g(\Delta\rho/\rho_\infty)L^3/\nu^2$ is the Grashof number, which has the form $G_r =(01\ s^2/cm)g$ in the present study, the ratio $\Delta\rho/\rho$ has the value of 0.01 in the present study, and $M_c = \Delta C\ L(d\xi/dC)/(D\mu)$ is the Marangoni number, where ξ is the surface tension and μ is the dynamic viscosity. For simplicity of notation all the non-dimensional variables, with the exception of solute concentration, are designated by the same symbols as those used for their dimensional form.

3. Computational Procedure

The numerical code used in the present investigation is a finite-difference Navier-Stokes code for non-staggered Cartesian grids. A colleague of the second author provided its original version.

Figure 1(b) presents the crystal growth system, computational grid and the boundary conditions used in the numerical simulation. The geometry of the two-dimensional

model is somewhat similar to the one used by Ramachandran et al. [28]. The upper surface of the fluid is a free boundary, which is assumed to be flat. All the other surfaces are no-slip walls. The grid details are shown in the figure 1b. After doing the required sensitivity tests, a grid of 88×97 was used throughout the simulations, with the grid lines clustered towards the walls. The code uses a finite-difference scheme in two-dimensional Cartesian coordinates on non-staggered grid. The convective terms were discretised using positive coefficient skew upwinding and for diffusive terms central differencing was used. The code was benchmarked with pure natural convection case and with the simulations in [28] and was found to give good agreement.

The case of $g=0.000001g_0$ is used as the baseline case for the simulations, and each case was run for several different angles of inclination γ. The parameters of interest are the maximum V_{max} of the magnitude of **u** in the protein growth system, which is also referred to as global maximum velocity, the Sherwood number S_h, and the local velocity V_{loc}, which is defined as the maximum value of the magnitude of velocity vector **u** in a domain of 2 non-dimensional units away from the crystal surface.

4. Results and Discussion

A discussion of the results obtained in the present investigation is as follows. Firstly, the results for the cases of $g= 0.000001g_0$ and $\gamma=0.0$ with the free surface level very close to the upper face of the crystal, where the non-dimensional perpendicular distance d between the free surface and the upper face of the crystal is taken the value of 0.074 and either M_c is zero or the effects of the surface tension driving force on the crystal growth can be significant for a given non-zero M_c, are presented and discussed in this and the following two paragraphs. Figure 2 presents results for $M_c=\gamma=0$. It shows the variations of the two velocity scales V_{max} and V_{loc} with respect to the Taylor number. It is seen that for very small values of the rotation rate, there is a slight decrease in the velocity scales, which is already very small (~0.00005 cm/s) after which the velocity increases sharply with the rotation rate. Thus it can be concluded that moderate and strong rotation can increase the convection at zero Marangoni number. The flow velocity contours and

vectors are visualized in Figure 3 for different $\sqrt{T_a}$, where the same trend is better seen. Our calculation results for the Sherwood number at these values of M_c and g indicate that S_h remain nearly a constant for the studied range of $\sqrt{T_a}$. Figure 4 shows the M_c=1000.0 and γ=0.0 results. Unlike the previous case where there was little difference between the maximum and local velocity scales, here the local velocity scales are significantly lower than the maximum velocity scales over most of the domain for $\sqrt{T_a}$ that have been investigated. In this case, it is seen that though the local velocity scale increases almost linearly with $\sqrt{T_a}$, the maximum velocity scale decreases for $\sqrt{T_a}$ in the range $0 \leq \sqrt{T_a} \leq 50.0$, after which it increases and for $\sqrt{T_a} > 80.0$ it becomes more than the local velocity scale. Our calculation results for the Sherwood number at these values of M_c and g (Figure 5) indicate that, as T_a increases from zero value, S_h decreases first and then increases monotonically, a minimum is reached at about $\sqrt{T_a}$=20.0. Here S_h is normalized with respect to its value in the absence of convection and $M_a \equiv M_c/S_c$ .The maximum velocity scale was also seen from the figure 4 that reaches a minimum value at this value of $\sqrt{T_a}$. It is to be noted that the values of the velocity scales are about 100.0 times more than the corresponding velocity scales values for the M_c=0.0 case, and the rotation rate required to bring a notable effect correspond to values of $\sqrt{T_a}$ about 10 times larger than the $\sqrt{T_a}$ values seen in the M_c=0.0 case.

The M_c =10000.0 case is considered next. The results for the local and maximum velocity scales presented in Figure 6 indicate that the values of these velocities are equal for zero rotation rate case, but with increasing $\sqrt{T_a}$, the local velocity scale decreases while the maximum velocity scale increases, reaches a peak at $\sqrt{T_a}$ about 25.0 and then begins to decrease. At $\sqrt{T_a}$ about 75.0 the minimum for both the maximum and local velocity scales are found, the minimum being almost 50% of the value at zero rotation. Further increase of $\sqrt{T_a}$ was found to increase the velocity scales only marginally. In Figure 7 the velocity contours and velocity vectors are visualized with increasing $\sqrt{T_a}$. The velocity vectors are seen at their maximum at the boundary, and these vectors are seen to shorten in length with increasing $\sqrt{T_a}$. Also the pattern of convection is seen. For small rotation rates, the convection is limited mainly to the left and right walls of the

crystal, in a counter clockwise direction on the left wall. With increasing $\sqrt{T_a}$, this convection is pushed upwards and new convection is seen to develop in the lower boundary of the crystal this one in a clockwise sense. The Sherwood number (figure 5) is seen to decrease by 50%, to a minimum at $\sqrt{T_a}$ corresponding to minimum velocity scales. The beneficial aspects of rotation are seen best for this case. The Sherwood number variation can be visualized by seeing Figure 8. There are steep gradients in the concentration for the low rotation case, but with increasing rotation, these contours are seen to spread out yielding lower S_h. When the contours are perfectly spread out as in the case of pure diffusion, the Sherwood number is minimized. Rotation is seen to drive the contours towards that ideal condition.

Figure 9 present the case of M_c=100000.0. Here the values of the velocity scales are about 1.5 cm/s or less. The maximum and local velocity scales decrease monotonically for increasing $\sqrt{T_a}$. For the highest $\sqrt{T_a}$ simulations, the maximum velocity scale is seen to equal the local velocity scale of 0.35, thus a decrease in the maximum velocity scale of about 4.2 times is seen. It is thus postulated that the beneficial effects of decreasing Marangoni convection is better for higher values of M_c. The results for S_h in this case and for cases of M_c=10000.0 and 1000.0 (figure 5) indicate that S_h increases with M_c.

Next, the results for the cases of $g=0.0001g_0$ and γ=0.0 with the free surface level again very close to the upper face of the crystal (d=0.074) are presented and discussed. We carried our computations to determine maximum and local velocity scales, Sherwood number, velocity contours, etc, for different M_c and $\sqrt{T_a}$ values and typical results for the velocity scales are presented in Figure 10 for M_c=10000.0. As can be seen from this figure, the maximum velocity scale is larger than the local velocity scale for zero rotation. As $\sqrt{T_a}$ increases beyond its zero value, both velocity scales decrease and reach a minimum value at about $\sqrt{T_a}$=100.0 beyond which the velocity scales increase strongly with the rotation rate. Larger values of g was found to require larger values of the rotation rate in order for the velocity scales to reach their minimum values. This result is consistent with the physical aspect of the destabilizing effects of the buoyancy force.

The effects of the location of the free surface relative to the location of the crystal were studied for cases where the free surface level was somewhat away by the distance d=1.486 parallel to the x-axis from the upper crystal face. We found that as d increases from the previously chosen value 0.074, then flow adjacent to the crystal face stabilizes as expected physically. Some typical results about the velocity vectors are presented in Figure 11 for $g=0.000001g_0$, $\gamma=0.0$, $M_c=10000.0$, d=1.486 and for several different values of $\sqrt{T_a}$. For small rotation, convection is seen to be limited to the region between the free surface and the crystal face parallel to the free surface and forming two circulations with opposite directions. With increasing $\sqrt{T_a}$, these flow circulations extend over the whole flow domain. We also generated data for velocity scales and the Sherwood number in this case but will not be presented in additional figures. Our additional calculated data for the Sherwood number in this case indicated qualitatively the same behavior as in the d=0.074 case, except that the minimum value of S_h occurs at a lower value of $\sqrt{T_a}$ if d is larger. Our results for the velocity scales indicated that the value of the local velocity scale decreases with increasing d, while the value of the maximum velocity scale increases with d for small rotation and slightly decreases with increasing d for large rotation.

In regard to the effect of the angle of inclination γ, we found that its effect on solute flux, local velocity scale and convection is generally not significant. However, its effect on the maximum velocity was found to be noticeable. For example, for $g=0.000001g_0$, $M_c=10000.0$ and $\sqrt{T_a}=120.0$, we found that the maximum velocity scale remains nearly a constant about 0.044 for γ less than about 30.0 degrees, while it increases with γ for $30.0° < \gamma \leq 90.0°$ reaching a maximum value of about 0.116 and then decreases with further increase in γ for $90.0° < \gamma \leq 165.0°$. For $165.0° < \gamma \leq 180.0°$, V_{max} again remains nearly a constant value of about 0.042.

5. Some Concluding Remarks

The results of the present investigation presented and discussed in the last section about the effects of inclined rotation on surface tension driven flow (Marangoni flow) during protein crystallization indicated that such flow can be weakened noticeably for the moderate rates of rotation, while such flow is can be enhanced for sufficiently large rotation rates. Further more, we found that stronger Marangoni flow can be weakend by applying rotation rate of larger magnitude and the effect of the angle of inclination γ on the Marangoni flow is rather weak in the present system. Unfortunately no experimental results are available at present for a rotating Marangoni flow during crystal growth in either micogravity or normal gravity environment in order to be able to make at least some comparison between the results of the present computational results and those due to the experimental observation. However, the present numerical results can stimulate experimental studies for further understanding the effects of rotation on such flows, which significantly dominate over buoyancy driven flows in a microgravity environment.

As can be seen from the non-dimensional form of the governing system given in the section 2, the centrifugal force appears to dominate over the Coriolis force for $T_a>1.0$, while the Coriolis force dominates over the centrifugal force for $0.0<T_a<1.0$. Since our results generally indicate that the Marangoni flow is weakest for a T_a value, which is generally larger than 1.0, we can conclude that in the regime for higher quality production of the protein crystals, centrigugal force dominates over the Coriolis force.

In regard to the insignificant effect of the angle of inclination γ on the Sherwood number and the convective flow in the vicinity of the crystal face detected in the present microgravity system, it should be noted that it may be related to the fact that here the surface tension gradient force dominates over the gravity force and the angle of inclination γ is the angle between the crystal axis and the rotation axis, which is either parallel or anti-parallel to the weak gravity force, so that both the magnitude and direction of the weak gravity force are insignificant in the present system.

Finally, it should be noted that, as partly explained earlier in the introduction section, the present protein crystal growth system is studied for a two-dimensional planar model and in microgravity environments only. It is quite possible that similar system could be studied experimentally in future first under normal gravity condition where both buoyancy and Marangoni forces are significant and the system actually is in three-dimension. Hence, it would be quite appropriate and interesting to investigate such a three-dimensional extension of our present study under both microgravity and normal gravity conditions in order to determine the results, which can be compared to possible future experimental data as well as to detect the possible beneficial roles that rotation can play to weaken either or both of the buoyancy and surface tension gradient forces.

Acknowledgement

This research was supported by the University of Illinois Research Board. The authors would like also to thank Dr. N. Ramachandran of Universities Space Research association for technical support and valuable comments on the subject.

References

[1] *Delucas, L. J., Smith, C. D., Smith, W., Vijay-Kumar, S., Senadhi, S. E., Ealick, S. E., Carter, D. C., Snyder, R. S., Weber, P. C., Raymond Salemme, F., OhAlendorf, D. H., Einspahr, H. M., Clancy, L. L., Navia, M. A., McKeever, B. M., Nagabhushan, T. L., Nelson,G., McPherson, A., Kozelak, S., Taylor,G., Stammers, D., Powel, K., Darby, G., Bugg, C. E.:* Protein Crystal Growth Results for Shuttle Flights. Journal of Crystal Growth, vol. 110, pp. 302-311 (1991).

[2] *Day, J., McPherson, A.:* Macromolecular Crystal Growth Experiments on International Microgravity Laboratory. Protein Science, vol. 1, pp. 1254-1268 (1992).

[3] *Delucas, L. J., Long, M. M., Moore, K. M., Rosenblum, W. M., Bray, T. L., Smith, C., Carson, M., Narayana, S. V. L., Harrington, M. D., Clark Jr., A, D., Nanni, R. G., Ding, J., Jacobo-Molina A., Kamer, G., Hughes, H. S., Arnold, E., Einspahr, H. M., Clancy, L. L., Rao, G. S. J., Cook, P. F., Harris, B. J., Munson, S. H., Finzel, B. C., McPherson, A., Weber, P. C., Lewandowski, F. A., Nagabhushan, T. L., Trotta, P. P., Reichert, P., Navia, M. A., Wilson, K. P., Thomson, J. A., Richards, R. N., Bowersox,*

K. D., Meade, C. J., Baker, E. S., Bishop, S. P., Dumbar, B. J., Trinh, E., Prahl, J., Sacco Jr., A., Bugg, C. E.: Recent Results and New Hardware Developments for Protein Crystal Growth in Microgravity. Journal of Crystal Growth, vol. 135, pp. 183-195 (1994).

[4] *Long, M. M., Delucas, L. J., Smith, C., Carson, M., Moore, K., Harrington, M. D., Pillion, D. J., Bishop, S. P., Rosenblum, W. M., Naumann, R. J., Chait, A., Prahl, J., Bugg, C. E.:* Protein Crystal Growth in Microgravity-Temperature induced Large Scale Crystallization of Insulin. Microgravity Science and Technology, vol. 7(2), pp. 196-202 (1994).

[5] *Lie, K. H., Walker, J. S., Riahi, D. N.:* Centrifugal pumping in a liquid cylinder in an axial magnetic field with application to semi-conductor crystal growth. Proceedings of the First Congress in Fluid Dynamics, vol. 3, pp. 2141-2147 (1988).

[6] *Lie, K. H., Walker, J. S., Riahi, D. N.:* Centrifugal pumping in the float-zone growth of silicon crystal with an axial magnetic field. Journal of Physico-Chemical Hydrodynamics, vol.10, pp. 441-460 (1988).

[7] *Riahi, D. N.:* Effects of centrifugal and Coriolis forces on chimney convection during alloy solidification. Journal of Crystal Growth, vol. 179, pp. 287-296 (1997).

[8] *Riahi, D. N.:* Effect of rotation on a non-axiymmetric chimney convection during alloy solidification. Journal of Crystal Growth, vol. 204, pp. 382-394 (1999).

[9] *Riahi, D. N.:* Effects of centrifugal and Coriolis forces on a hydromagnetic chimney convection in a mushy layer. Journal of Crystal Growth, vol. 226, pp. 393-405 (2001).

[10] *Davis, S. H.:* Thermocapillary Instabilities. Annual Review of Fluid Mechanics, vol. 19, pp. 403-435 (1987).

[11] *Scanlon, J., Segel, L.*: Finite Amplitude Cellular Convection Induced by Surface Tension. Journal of Fluid Mechanics, vol. 30, pp. 149-162 (1967).

[12] *Lebon, G., Cloot, A.:* Buoyancy and Surface Tension Driven Instabilities in Presence of Negative Rayleigh and Marangoni Numbers. Acta Mechanica, vol. 43, pp. 141-158 (1982).

[13] *Lebon, G., Cloot, A.:* A Nonlinear Stability Analysis of the Benard-Marangoni Problem. Journal of Fluid Mechanics, vol. 145, pp. 447-469 (1984).

[14] *Riahi, D. N.:* Thermocapillary Instability of an Infinite Prandtl Number Fluid with Negligible Gravitational Effects. Acta Mechanica, vol. 64, pp. 155-163 (1986).

[15] *Riahi, D. N.:* Nonlinear Benard-Marangoni Convection. Journal of the Physical Society of Japan, vol. 56, pp. 3515-3524 (1987).

[16] *Riahi, D. N.:* Thermocapillary Instability of a Low Prandtl Number Fluid with Negligible Gravitational Effects. Acta Mechanica, vol. 71, pp. 249-252 (1988).

[17] *Riahi, D. N.:* Hexagon Pattern Convection for Benard-Marangoni Problem. International Journal of Engineering Sciences, vol. 27, pp. 689-700 (1989).

[18] *Ramachandran, N.:* Thermal Buoyancy and Marangoni Convection in a Two Fluid Layered System. Journal of Thermophysics and Heat Transfer, vol. 7, pp. 352-360 (1993).

[19] *Kliakhandler, I. L., Nepomnyashchy, A. A., Simanovski, I. B., Zaks, M. A.:* Nonlinear Marangoni waves in Multilayer System. Physical Review E, vol. 58, pp. 5765-5775 (1998).

[20] *Bragard, J., Velarde, M. G.:* Benard-Marangoni Convection: Planforms and Related Theoretical Predictions. Journal of Fluid Mechanics, vol. 368, pp. 165-194 (1998).

[21] *Riahi, D. N.:* Nonlinear Benard-Marangoni Convection in a Rotating Layer. Letters in Applied and Engineering Sciences, vol. 32, pp. 877-882 (1994).

[22] *Riahi, D. N., Walker, J. S.:* Nonlinear Thermocapillary Convection in a Liquid Cylinder. Proceedings of the First Congress in Fluid Dynamics, vol. 3, pp. 1908-1913 (1988).

[23] *Lie, K. H., Riahi, D. N., Walker, J. S.:* Buoyancy and Surface Tension Driven Flows in Float Zone Crystal Growth with a Strong Axial Magnetic Field. International Journal of Heat and Mass Transfer, vol. 32, pp. 2409-2420 (1989).

[24] *Molenkamp, T.:* Marangoni Convection, Mass Transfer and Microgravity. Thesis. The Dutch Experiment Support Center (1998).

[25] *Rosenberger, F.:* Inorganic and Protein Crystal Growth. Journal of Crystal Growth, vol. 76, pp. 618-636 (1986).

[26] *Monti, R., Savino, R.:* Fluid-Dynamic Modelling of Protein Crystallizers, in: Materials and Fluids Under Low Gravity. Ratke, L., Walter, H., Feuerbacher, B. (Eds.), Springer-Verlag, Berlin, pp. 171-194 (1996).

[27] *Monti, R., Savino, R.:* Buoyancy and Surface-Tension-Driven Convection in a Hanging Drop Protein Crystallizer. Journal of Crystal Growth, vol. 165, pp. 308-318 (1996).

[28] *Ramachandran, N., Baugher, C. R., Naumann, R. J.:* Modeling Flows and Transport in Protein Crystal Growth. Microgravity Science and Technology, vol. 8(3), pp. 170-179 (1995).

[29] *Chandrasekhar, S.:* Hydrodynamic and Hydromagnetic Stability. Clarendon Press, Oxford, (1961).

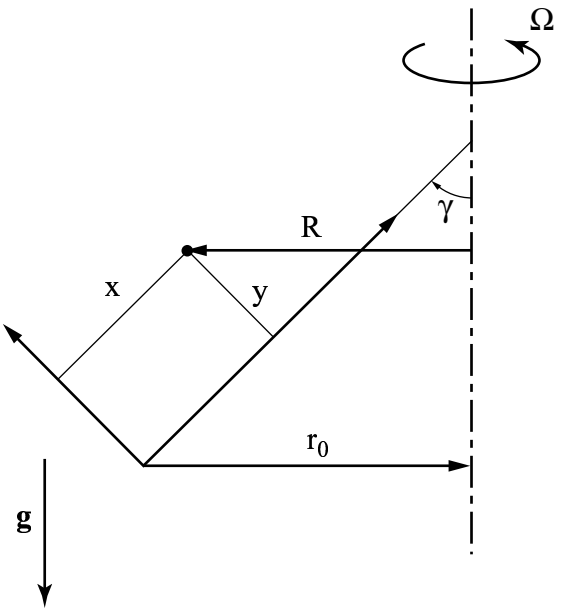

(a)

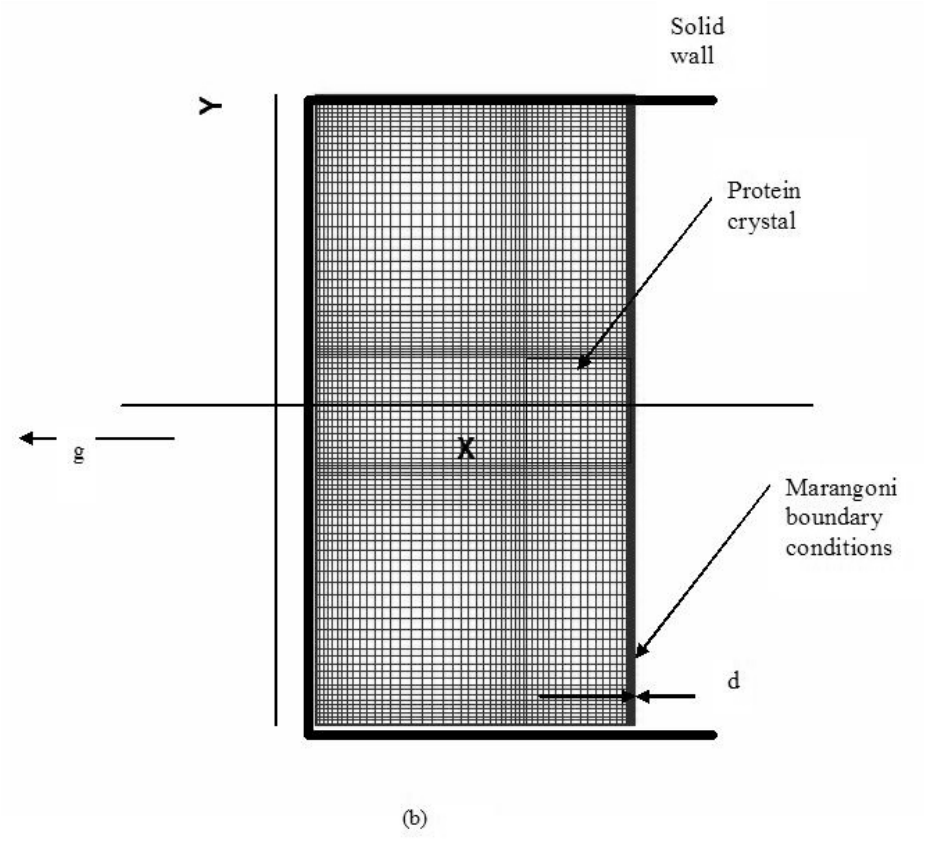

(b)

Figure 1. (a) Planar geometry and the coordinates for the crystal growth system. (b) Computational grid and boundary conditions.

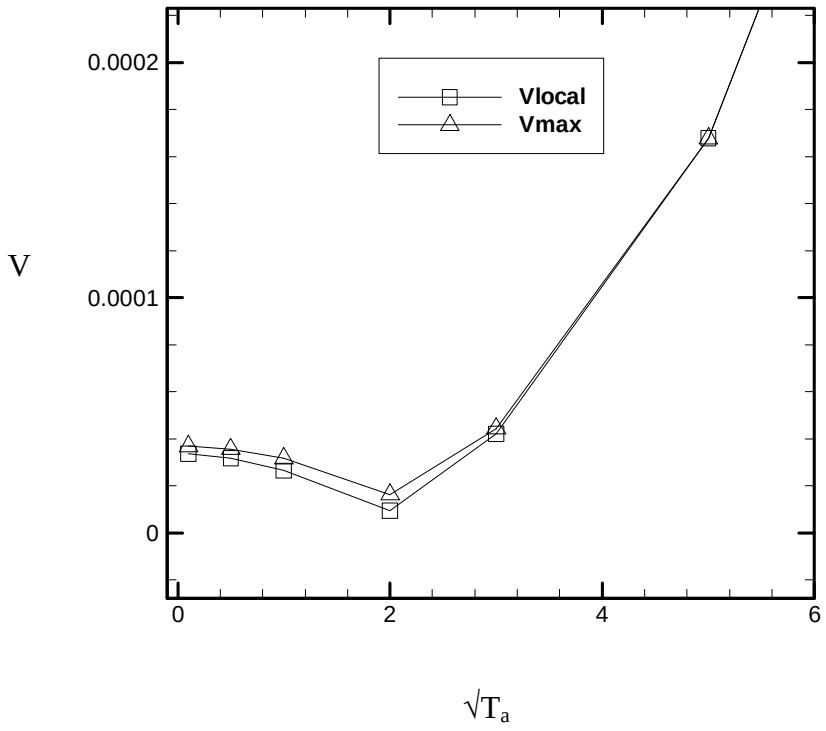

Figure 2. Local and maximum velocity scales versus $\sqrt{T_a}$ for $g=0.000001g_0$ and $M_c=0.0$.

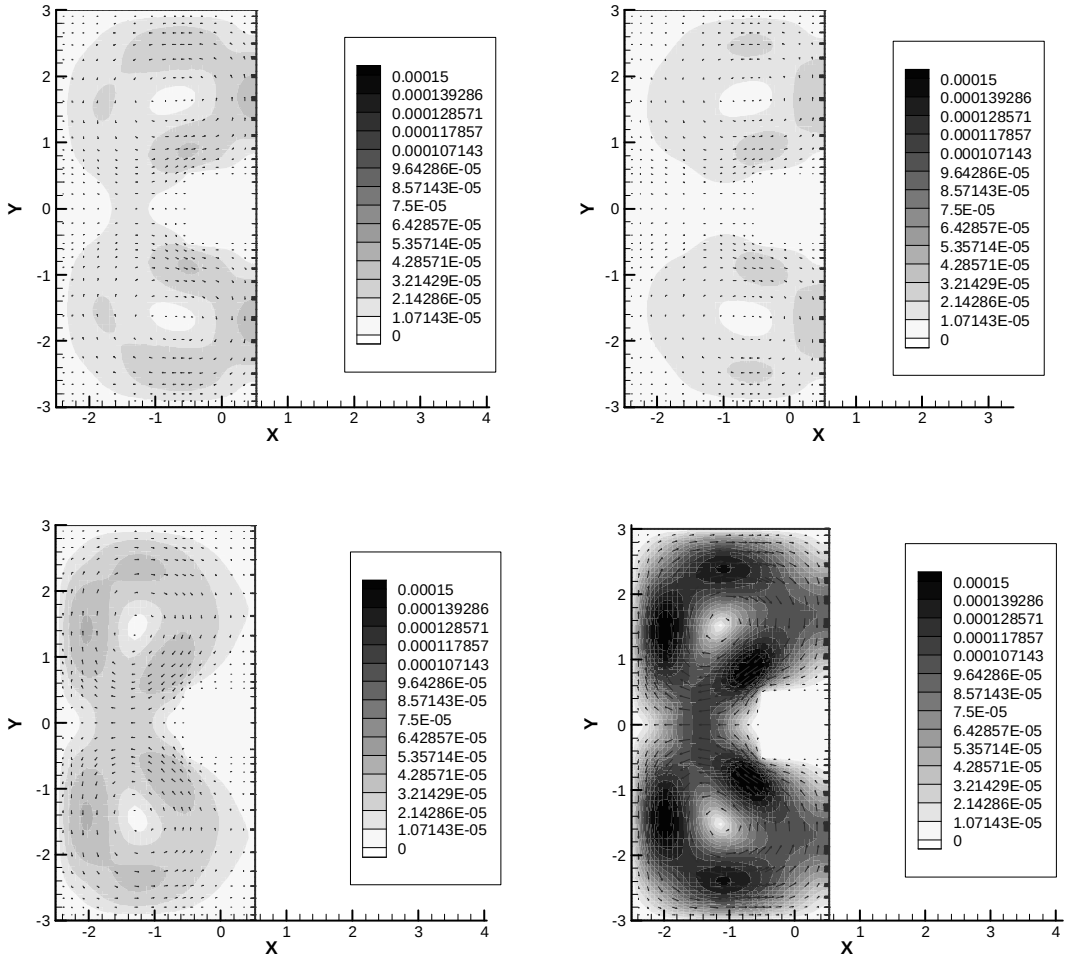

Figure 3. Total velocity contours and velocity vectors ($g=0.000001g_0$ and $M_c=0.0$) for $\sqrt{T_a}$ = 0.2 (upper left), 2.0 (upper right), 3.0 (lower left) and 6.0 (lower right). Here K denotes the magnitude of the velocity vector.

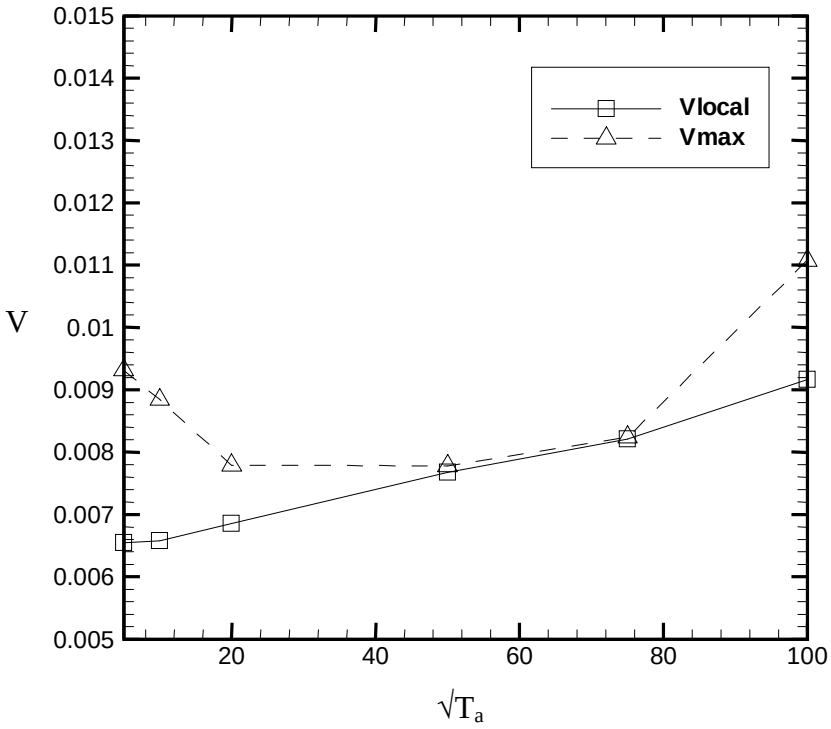

Figure 4. Local and maximum velocity scales versus $\sqrt{T_a}$ for $g=0.000001g_0$ and $M_c=1000$.

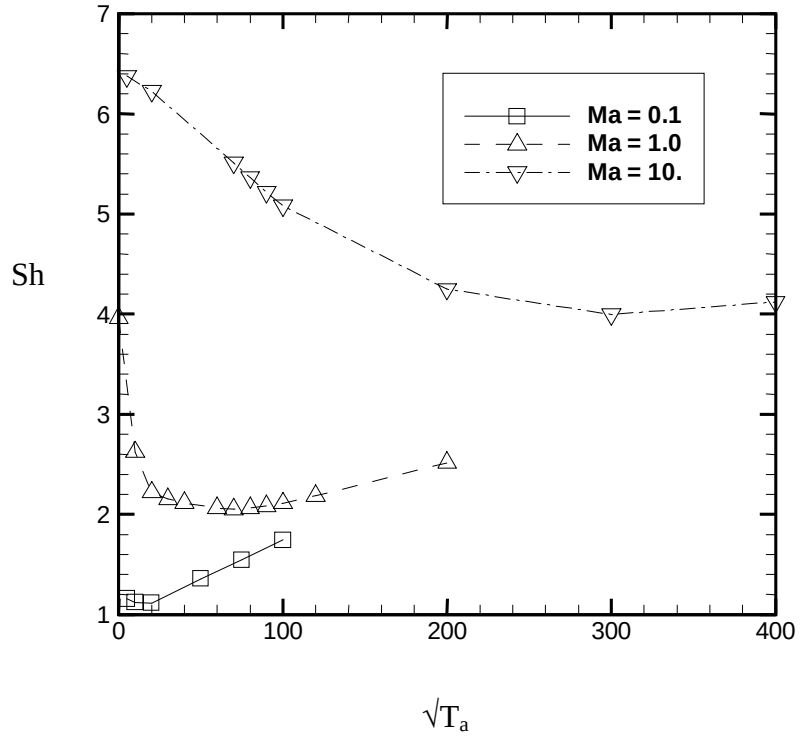

Figure 5. Sherwood number versus $\sqrt{T_a}$ ($g=0.000001g_0$) for M_a (M_c /10000.0) =0.1, 1.0 and 10.0.

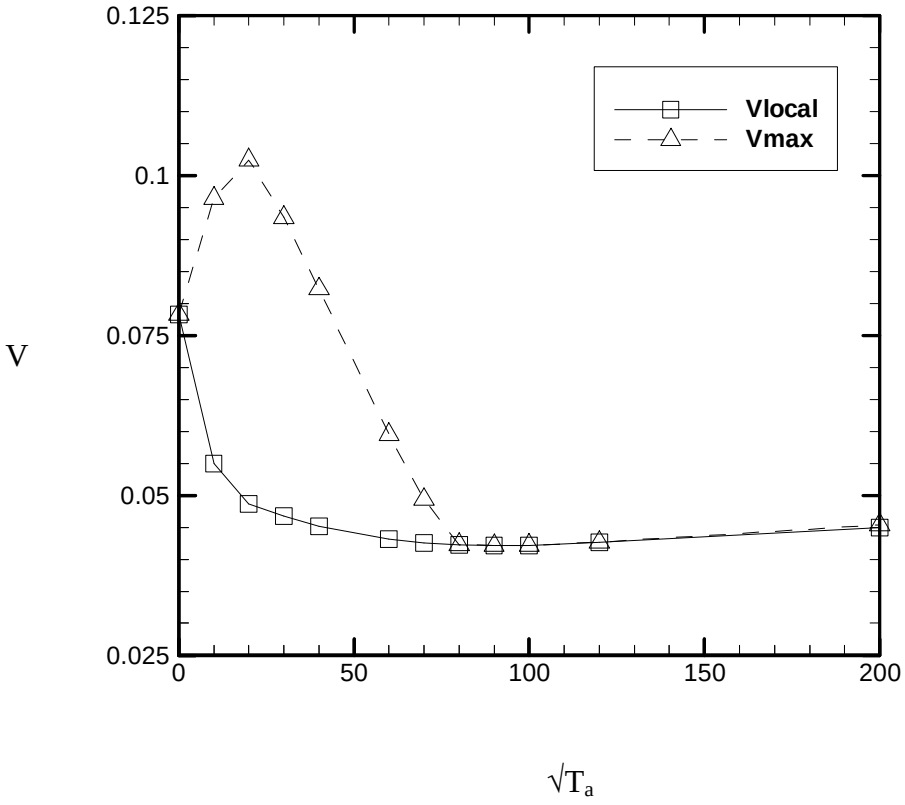

Figure 6. Local and maximum velocity scales versus $\sqrt{T_a}$ for $g=0.000001g_0$ and M_c =10000.0.

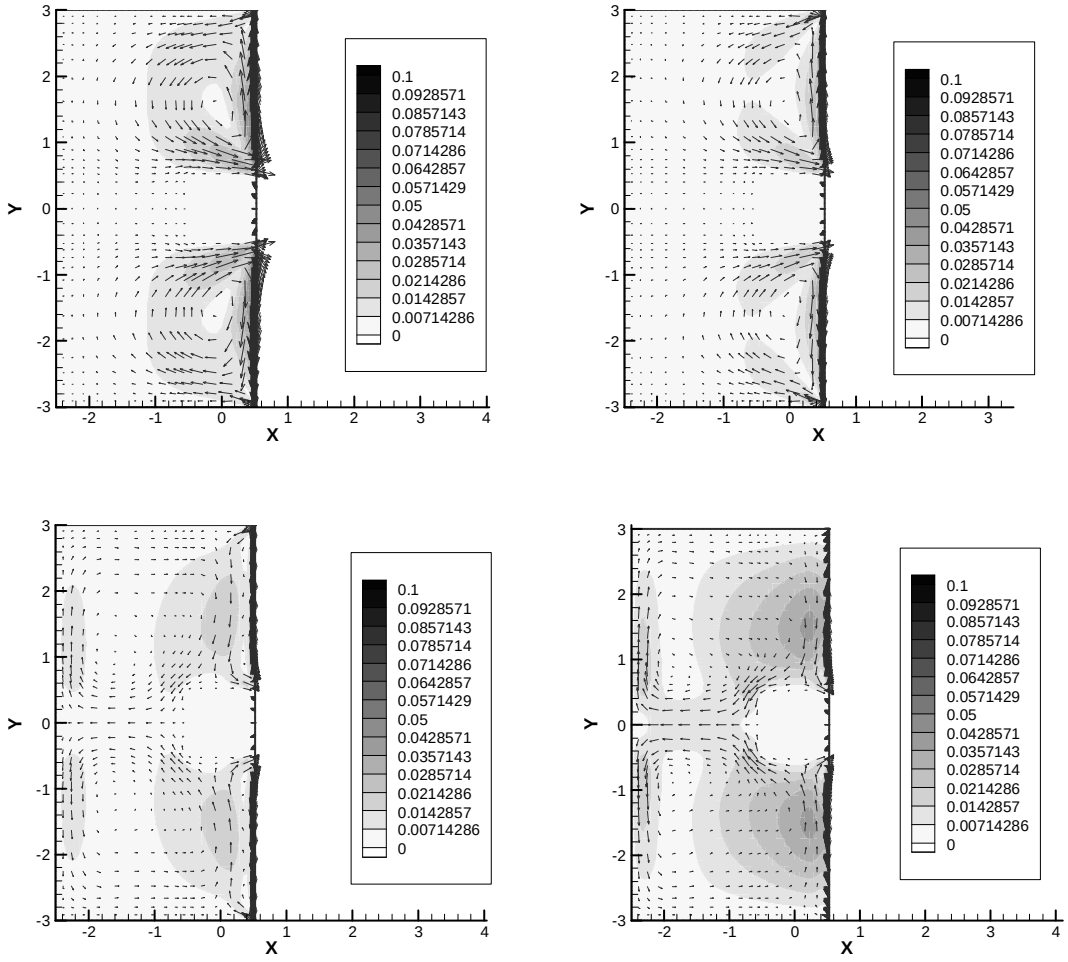

Figure 7. Total velocity contours and velocity vectors ($g=0.000001g_0$ and $M_c=10000.0$) for $\sqrt{T_a}=5.0$ (upper left), 20.0 (upper right), 40.0 (lower left) and 100.0 (lower right).

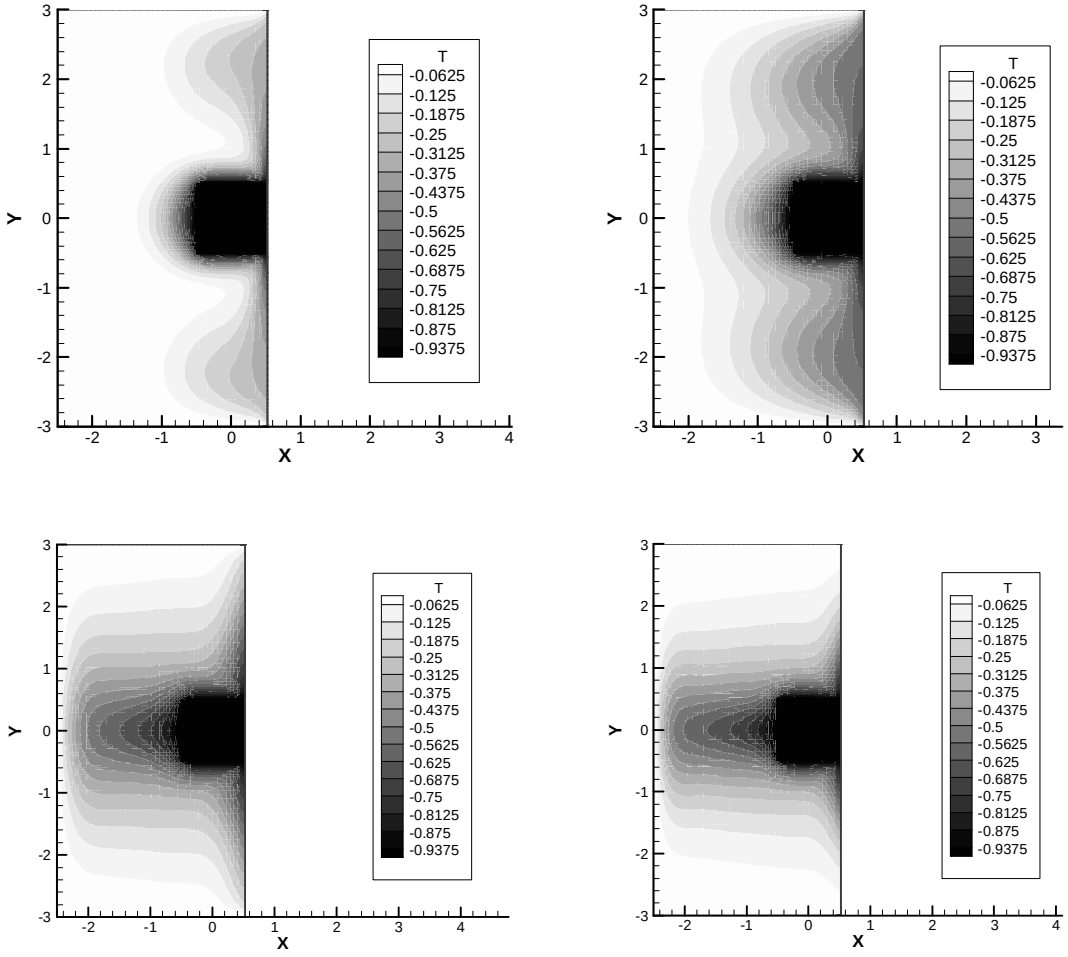

Figure 8. Concentration contours ($g=0.000001g_0$ and $M_c=10000.0$) for $\sqrt{T_a}=5.0$ (upper left), 20.0 (upper right), 40.0 (lower left) and 100.0 (lower right). Here T denotes iso-concentration value.

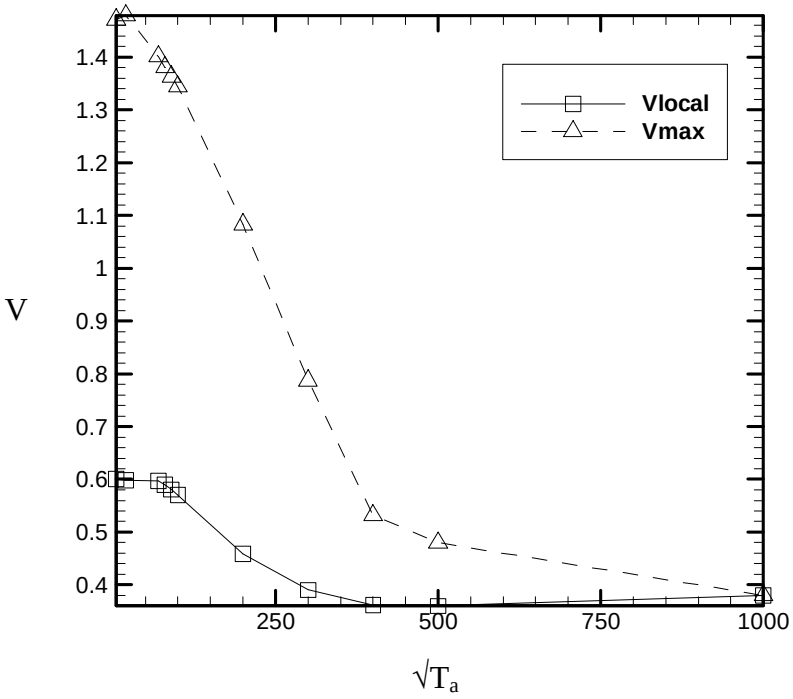

Figure 9. Local and maximum velocity scales versus $\sqrt{T_a}$ for $g=0.000001g_0$ and $M_c=100000.0$).

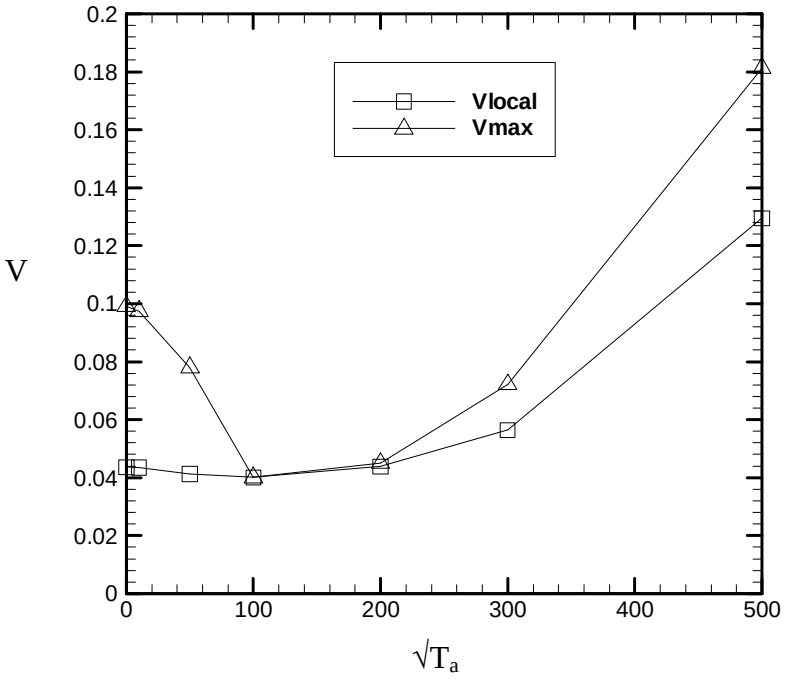

Figure 10. Local and maximum velocity scales versus $\sqrt{T_a}$ for $g=0.0001g_0$ and M_c =10000.0.

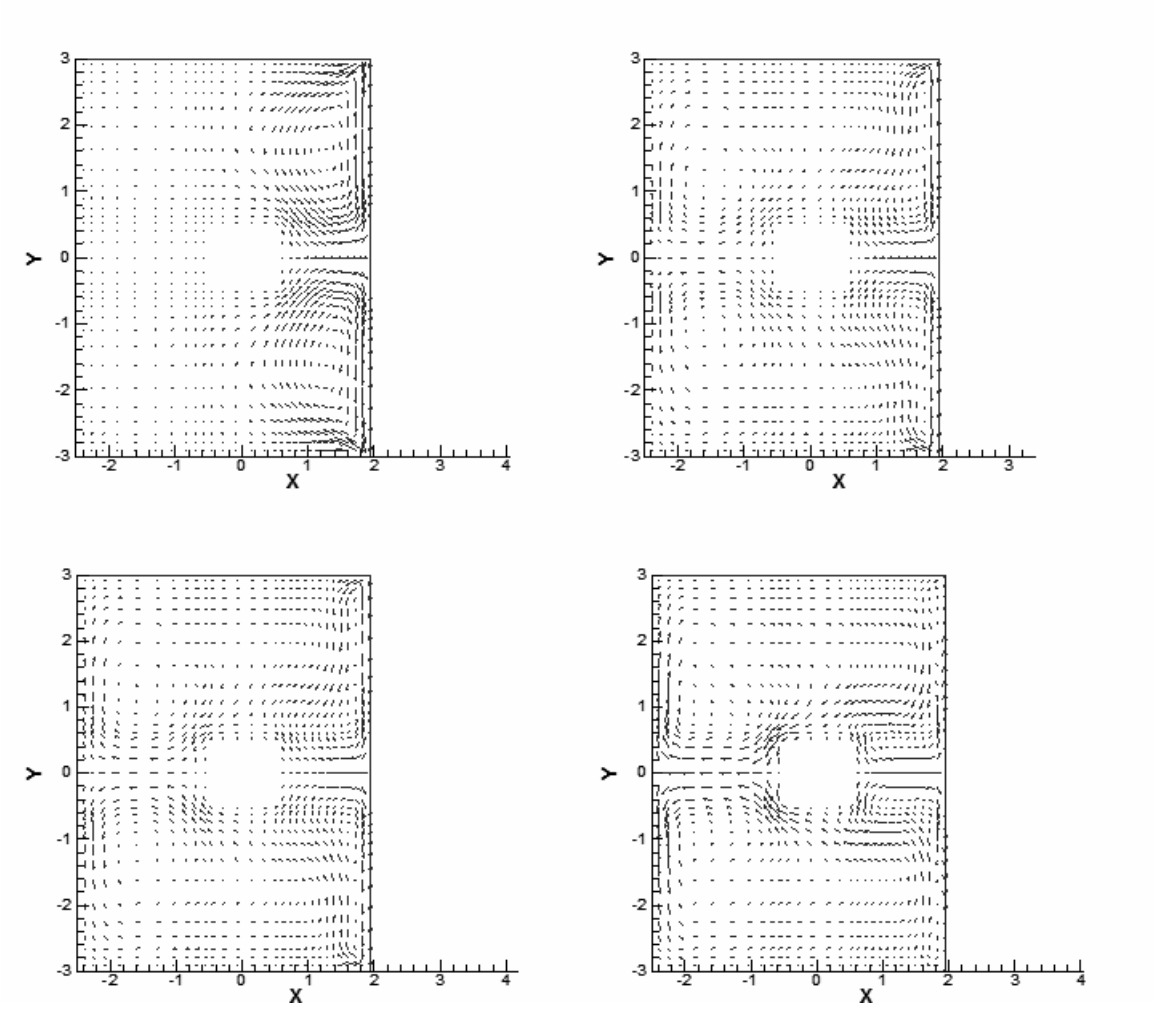

Figure 11. Velocity vectors ($g=0.00001g_0$, $M_c=10000.0$, $d=1.486$) for $\sqrt{T_a}$ =5.0 (upper left), 20.0 (upper right), 40.0 (lower left) and 100.0 (lower right).

List of Recent TAM Reports

No.	Authors	Title	Date
935	Hsui, A. T., and D. N. Riahi	Onset of thermal–chemical convection with crystallization within a binary fluid and its geological implications—*Geochemistry, Geophysics, Geosystems* **2**, 2000GC000075 (2001)	Apr. 2000
936	Cermelli, P., E. Fried, and S. Sellers	Configurational stress, yield, and flow in rate-independent plasticity—*Proceedings of the Royal Society of London A* **457**, 1447–1467 (2001)	Apr. 2000
937	Adrian, R. J., C. Meneveau, R. D. Moser, and J. J. Riley	Final report on 'Turbulence Measurements for Large-Eddy Simulation' workshop	Apr. 2000
938	Bagchi, P., and S. Balachandar	Linearly varying ambient flow past a sphere at finite Reynolds number—Part 1: Wake structure and forces in steady straining flow	Apr. 2000
939	Gioia, G., A. DeSimone, M. Ortiz, and A. M. Cuitiño	Folding energetics in thin-film diaphragms—*Proceedings of the Royal Society of London A* **458**, 1223–1229 (2002)	Apr. 2000
940	Chaïeb, S., and G. H. McKinley	Mixing immiscible fluids: Drainage induced cusp formation	May 2000
941	Thoroddsen, S. T., and A. Q. Shen	Granular jets—*Physics of Fluids* **13**, 4–6 (2001)	May 2000
942	Riahi, D. N.	Non-axisymmetric chimney convection in a mushy layer under a high-gravity environment—In *Centrifugal Materials Processing* (L. L. Regel and W. R. Wilcox, eds.), 295–302 (2001)	May 2000
943	Christensen, K. T., S. M. Soloff, and R. J. Adrian	PIV Sleuth: Integrated particle image velocimetry interrogation/validation software	May 2000
944	Wang, J., N. R. Sottos, and R. L. Weaver	Laser induced thin film spallation—*Experimental Mechanics* (submitted)	May 2000
945	Riahi, D. N.	Magnetohydrodynamic effects in high gravity convection during alloy solidification—In *Centrifugal Materials Processing* (L. L. Regel and W. R. Wilcox, eds.), 317–324 (2001)	June 2000
946	Gioia, G., Y. Wang, and A. M. Cuitiño	The energetics of heterogeneous deformation in open-cell solid foams—*Proceedings of the Royal Society of London A* **457**, 1079–1096 (2001)	June 2000
947	Kessler, M. R., and S. R. White	Self-activated healing of delamination damage in woven composites—*Composites A: Applied Science and Manufacturing* **32**, 683–699 (2001)	June 2000
948	Phillips, W. R. C.	On the pseudomomentum and generalized Stokes drift in a spectrum of rotational waves—*Journal of Fluid Mechanics* **430**, 209–229 (2001)	July 2000
949	Hsui, A. T., and D. N. Riahi	Does the Earth's nonuniform gravitational field affect its mantle convection?—*Physics of the Earth and Planetary Interiors* (submitted)	July 2000
950	Phillips, J. W.	Abstract Book, 20th International Congress of Theoretical and Applied Mechanics (27 August – 2 September, 2000, Chicago)	July 2000
951	Vainchtein, D. L., and H. Aref	Morphological transition in compressible foam—*Physics of Fluids* **13**, 2152–2160 (2001)	July 2000
952	Chaïeb, S., E. Sato-Matsuo, and T. Tanaka	Shrinking-induced instabilities in gels	July 2000
953	Riahi, D. N., and A. T. Hsui	A theoretical investigation of high Rayleigh number convection in a nonuniform gravitational field—*International Journal of Pure and Applied Mathematics*, in press (2003)	Aug. 2000
954	Riahi, D. N.	Effects of centrifugal and Coriolis forces on a hydromagnetic chimney convection in a mushy layer—*Journal of Crystal Growth* **226**, 393–405 (2001)	Aug. 2000
955	Fried, E.	An elementary molecular-statistical basis for the Mooney and Rivlin–Saunders theories of rubber-elasticity—*Journal of the Mechanics and Physics of Solids* **50**, 571–582 (2002)	Sept. 2000

List of Recent TAM Reports (cont'd)

No.	Authors	Title	Date
956	Phillips, W. R. C.	On an instability to Langmuir circulations and the role of Prandtl and Richardson numbers—*Journal of Fluid Mechanics* **442**, 335–358 (2001)	Sept. 2000
957	Chaïeb, S., and J. Sutin	Growth of myelin figures made of water soluble surfactant—Proceedings of the 1st Annual International IEEE–EMBS Conference on Microtechnologies in Medicine and Biology (October 2000, Lyon, France), 345–348	Oct. 2000
958	Christensen, K. T., and R. J. Adrian	Statistical evidence of hairpin vortex packets in wall turbulence—*Journal of Fluid Mechanics* **431**, 433–443 (2001)	Oct. 2000
959	Kuznetsov, I. R., and D. S. Stewart	Modeling the thermal expansion boundary layer during the combustion of energetic materials—*Combustion and Flame*, in press (2001)	Oct. 2000
960	Zhang, S., K. J. Hsia, and A. J. Pearlstein	Potential flow model of cavitation-induced interfacial fracture in a confined ductile layer—*Journal of the Mechanics and Physics of Solids*, **50**, 549–569 (2002)	Nov. 2000
961	Sharp, K. V., R. J. Adrian, J. G. Santiago, and J. I. Molho	Liquid flows in microchannels—Chapter 6 of *CRC Handbook of MEMS* (M. Gad-el-Hak, ed.) (2001)	Nov. 2000
962	Harris, J. G.	Rayleigh wave propagation in curved waveguides—*Wave Motion* **36**, 425–441 (2002)	Jan. 2001
963	Dong, F., A. T. Hsui, and D. N. Riahi	A stability analysis and some numerical computations for thermal convection with a variable buoyancy factor—*Journal of Theoretical and Applied Mechanics* **2**, 19–46 (2002)	Jan. 2001
964	Phillips, W. R. C.	Langmuir circulations beneath growing or decaying surface waves—*Journal of Fluid Mechanics* (submitted)	Jan. 2001
965	Bdzil, J. B., D. S. Stewart, and T. L. Jackson	Program burn algorithms based on detonation shock dynamics—*Journal of Computational Physics* (submitted)	Jan. 2001
966	Bagchi, P., and S. Balachandar	Linearly varying ambient flow past a sphere at finite Reynolds number: Part 2—Equation of motion—*Journal of Fluid Mechanics* (submitted)	Feb. 2001
967	Cermelli, P., and E. Fried	The evolution equation for a disclination in a nematic fluid—*Proceedings of the Royal Society A* **458**, 1–20 (2002)	Apr. 2001
968	Riahi, D. N.	Effects of rotation on convection in a porous layer during alloy solidification—Chapter 12 in *Transport Phenomena in Porous Media* (D. B. Ingham and I. Pop, eds.), 316–340 (2002)	Apr. 2001
969	Damljanovic, V., and R. L. Weaver	Elastic waves in cylindrical waveguides of arbitrary cross section—*Journal of Sound and Vibration* (submitted)	May 2001
970	Gioia, G., and A. M. Cuitiño	Two-phase densification of cohesive granular aggregates—*Physical Review Letters* **88**, 204302 (2002) (in extended form and with added co-authors S. Zheng and T. Uribe)	May 2001
971	Subramanian, S. J., and P. Sofronis	Calculation of a constitutive potential for isostatic powder compaction—*International Journal of Mechanical Sciences* (submitted)	June 2001
972	Sofronis, P., and I. M. Robertson	Atomistic scale experimental observations and micromechanical/continuum models for the effect of hydrogen on the mechanical behavior of metals—*Philosophical Magazine* (submitted)	June 2001
973	Pushkin, D. O., and H. Aref	Self-similarity theory of stationary coagulation—*Physics of Fluids* **14**, 694–703 (2002)	July 2001
974	Lian, L., and N. R. Sottos	Stress effects in ferroelectric thin films—*Journal of the Mechanics and Physics of Solids* (submitted)	Aug. 2001
975	Fried, E., and R. E. Todres	Prediction of disclinations in nematic elastomers—*Proceedings of the National Academy of Sciences* **98**, 14773–14777 (2001)	Aug. 2001
976	Fried, E., and V. A. Korchagin	Striping of nematic elastomers—*International Journal of Solids and Structures* **39**, 3451–3467 (2002)	Aug. 2001

List of Recent TAM Reports (cont'd)

No.	Authors	Title	Date
977	Riahi, D. N.	On nonlinear convection in mushy layers: Part I. Oscillatory modes of convection—*Journal of Fluid Mechanics* **467**, 331–359 (2002)	Sept. 2001
978	Sofronis, P., I. M. Robertson, Y. Liang, D. F. Teter, and N. Aravas	Recent advances in the study of hydrogen embrittlement at the University of Illinois—Invited paper, Hydrogen–Corrosion Deformation Interactions (Sept. 16–21, 2001, Jackson Lake Lodge, Wyo.)	Sept. 2001
979	Fried, E., M. E. Gurtin, and K. Hutter	A void-based description of compaction and segregation in flowing granular materials—*Proceedings of the Royal Society of London A* (submitted)	Sept. 2001
980	Adrian, R. J., S. Balachandar, and Z.-C. Liu	Spanwise growth of vortex structure in wall turbulence—*Korean Society of Mechanical Engineers International Journal* **15**, 1741–1749 (2001)	Sept. 2001
981	Adrian, R. J.	Information and the study of turbulence and complex flow—*Japanese Society of Mechanical Engineers Journal B*, in press (2002)	Oct. 2001
982	Adrian, R. J., and Z.-C. Liu	Observation of vortex packets in direct numerical simulation of fully turbulent channel flow—*Journal of Visualization*, in press (2002)	Oct. 2001
983	Fried, E., and R. E. Todres	Disclinated states in nematic elastomers—*Journal of the Mechanics and Physics of Solids* **50**, 2691–2716 (2002)	Oct. 2001
984	Stewart, D. S.	Towards the miniaturization of explosive technology—Proceedings of the 23rd International Conference on Shock Waves (2001)	Oct. 2001
985	Kasimov, A. R., and Stewart, D. S.	Spinning instability of gaseous detonations—*Journal of Fluid Mechanics* (submitted)	Oct. 2001
986	Brown, E. N., N. R. Sottos, and S. R. White	Fracture testing of a self-healing polymer composite—*Experimental Mechanics* (submitted)	Nov. 2001
987	Phillips, W. R. C.	Langmuir circulations—*Surface Waves* (J. C. R. Hunt and S. Sajjadi, eds.), in press (2002)	Nov. 2001
988	Gioia, G., and F. A. Bombardelli	Scaling and similarity in rough channel flows—*Physical Review Letters* **88**, 014501 (2002)	Nov. 2001
989	Riahi, D. N.	On stationary and oscillatory modes of flow instabilities in a rotating porous layer during alloy solidification—*Journal of Porous Media*, in press (2002)	Nov. 2001
990	Okhuysen, B. S., and D. N. Riahi	Effect of Coriolis force on instabilities of liquid and mushy regions during alloy solidification—*Physics of Fluids* (submitted)	Dec. 2001
991	Christensen, K. T., and R. J. Adrian	Measurement of instantaneous Eulerian acceleration fields by particle-image accelerometry: Method and accuracy—*Experimental Fluids* (submitted)	Dec. 2001
992	Liu, M., and K. J. Hsia	Interfacial cracks between piezoelectric and elastic materials under in-plane electric loading—*Journal of the Mechanics and Physics of Solids* **51**, 921–944 (2003)	Dec. 2001
993	Panat, R. P., S. Zhang, and K. J. Hsia	Bond coat surface rumpling in thermal barrier coatings—*Acta Materialia* **51**, 239–249 (2003)	Jan. 2002
994	Aref, H.	A transformation of the point vortex equations—*Physics of Fluids* **14**, 2395–2401 (2002)	Jan. 2002
995	Saif, M. T. A, S. Zhang, A. Haque, and K. J. Hsia	Effect of native Al_2O_3 on the elastic response of nanoscale aluminum films—*Acta Materialia* **50**, 2779–2786 (2002)	Jan. 2002
996	Fried, E., and M. E. Gurtin	A nonequilibrium theory of epitaxial growth that accounts for surface stress and surface diffusion—*Journal of the Mechanics and Physics of Solids*, in press (2002)	Jan. 2002
997	Aref, H.	The development of chaotic advection—*Physics of Fluids* **14**, 1315–1325 (2002); see also *Virtual Journal of Nanoscale Science and Technology*, 11 March 2002	Jan. 2002
998	Christensen, K. T., and R. J. Adrian	The velocity and acceleration signatures of small-scale vortices in turbulent channel flow—*Journal of Turbulence*, in press (2002)	Jan. 2002

List of Recent TAM Reports (cont'd)

No.	*Authors*	*Title*	*Date*
999	Riahi, D. N.	Flow instabilities in a horizontal dendrite layer rotating about an inclined axis—*Proceedings of the Royal Society of London A* (submitted)	Feb. 2002
1000	Kessler, M. R., and S. R. White	Cure kinetics of ring-opening metathesis polymerization of dicyclopentadiene—*Journal of Polymer Science A* **40**, 2373–2383 (2002)	Feb. 2002
1001	Dolbow, J. E., E. Fried, and A. Q. Shen	Point defects in nematic gels: The case for hedgehogs—*Proceedings of the National Academy of Sciences* (submitted)	Feb. 2002
1002	Riahi, D. N.	Nonlinear steady convection in rotating mushy layers—*Journal of Fluid Mechanics*, in press (2003)	Mar. 2002
1003	Carlson, D. E., E. Fried, and S. Sellers	The totality of soft-states in a neo-classical nematic elastomer—*Proceedings of the Royal Society A* (submitted)	Mar. 2002
1004	Fried, E., and R. E. Todres	Normal-stress differences and the detection of disclinations in nematic elastomers—*Journal of Polymer Science B: Polymer Physics* **40**, 2098–2106 (2002)	June 2002
1005	Fried, E., and B. C. Roy	Gravity-induced segregation of cohesionless granular mixtures—*Lecture Notes in Mechanics*, in press (2002)	July 2002
1006	Tomkins, C. D., and R. J. Adrian	Spanwise structure and scale growth in turbulent boundary layers—*Journal of Fluid Mechanics* (submitted)	Aug. 2002
1007	Riahi, D. N.	On nonlinear convection in mushy layers: Part 2. Mixed oscillatory and stationary modes of convection—*Journal of Fluid Mechanics* (submitted)	Sept. 2002
1008	Aref, H., P. K. Newton, M. A. Stremler, T. Tokieda, and D. L. Vainchtein	Vortex crystals—*Advances in Applied Mathematics* **39**, in press (2002)	Oct. 2002
1009	Bagchi, P., and S. Balachandar	Effect of turbulence on the drag and lift of a particle—*Physics of Fluids* (submitted)	Oct. 2002
1010	Zhang, S., R. Panat, and K. J. Hsia	Influence of surface morphology on the adhesive strength of aluminum/epoxy interfaces—*Journal of Adhesion Science and Technology* (submitted)	Oct. 2002
1011	Carlson, D. E., E. Fried, and D. A. Tortorelli	On internal constraints in continuum mechanics—*Journal of Elasticity* (submitted)	Oct. 2002
1012	Boyland, P. L., M. A. Stremler, and H. Aref	Topological fluid mechanics of point vortex motions—*Physica D* **175**, 69–95 (2002)	Oct. 2002
1013	Bhattacharjee, P., and D. N. Riahi	Computational studies of the effect of rotation on convection during protein crystallization—*Journal of Crystal Growth* (submitted)	Feb. 2003
1014	Brown, E. N., M. R. Kessler, N. R. Sottos, and S. R. White	*In situ* poly(urea-formaldehyde) microencapsulation of dicyclopentadiene—*Journal of Microencapsulation* (submitted)	Feb. 2003
1015	Brown, E. N., S. R. White, and N. R. Sottos	Microcapsule induced toughening in a self-healing polymer composite—*Journal of Materials Science* (submitted)	Feb. 2003
1016	Kuznetsov, I. R., and D. S. Stewart	Burning rate of energetic materials with thermal expansion—*Combustion and Flame* (submitted)	Mar. 2003
1017	Dolbow, J., E. Fried, and H. Ji	Chemically induced swelling of hydrogels—*Journal of the Mechanics and Physics of Solids* (submitted)	Mar. 2003
1018	Costello, G. A.	Mechanics of wire rope—Mordica Lecture, Interwire 2003, Wire Association International, Atlanta, Georgia, May 12, 2003	Mar. 2003
1019	Wang, J., N. R. Sottos, and R. L. Weaver	Thin film adhesion measurement by laser induced stress waves—*Journal of the Mechanics and Physics of Solids* (submitted)	Apr. 2003
1020	Bhattacharjee, P., and D. N. Riahi	Effect of rotation on surface tension driven flow during protein crystallization—*Microgravity Science and Technology* (submitted)	Apr. 2003